METRICA
METRology Institutional CAtalog

ISTITUTO NAZIONALE DI RICERCA METROLOGICA
Repository Istituzionale

Effect of Low Copper Doping on the Optical, Cytocompatible, Antibacterial, and SARS-CoV-2 Trapping Properties of Calcium Phosphate Glasses

Original
Effect of Low Copper Doping on the Optical, Cytocompatible, Antibacterial, and SARS-CoV-2 Trapping Properties of Calcium Phosphate Glasses / Restivo, Elisa; Pugliese, Diego; Gallichi-Nottiani, Duccio; Sammartino, José Camilla; Bloise, Nora; Peluso, Emanuela; Percivalle, Elena; Janner, Davide; Milanese, Daniel; Visai, Livia. - In: ACS OMEGA. - ISSN 2470-1343. - 8:45(2023), pp. 42264-42274. [10.1021/acsomega.3c04293]
Availability:
This version is available at: 11696/78219 since: 2023-11-24T09:13:25Z

Publisher:
American Chemical Society

Published
DOI:10.1021/acsomega.3c04293

Terms of use:

This article is made available under terms and conditions as specified in the corresponding bibliographic description in the repository

Publisher copyright

(Article begins on next page)

25 November 2024

ACS OMEGA

Open Access

This article is licensed under CC-BY-NC-ND 4.0

http://pubs.acs.org/journal/acsodf

Article

Effect of Low Copper Doping on the Optical, Cytocompatible, Antibacterial, and SARS-CoV-2 Trapping Properties of Calcium Phosphate Glasses

Elisa Restivo, Diego Pugliese, Duccio Gallichi-Nottiani, José Camilla Sammartino, Nora Bloise, Emanuela Peluso, Elena Percivalle, Davide Janner,* Daniel Milanese,* and Livia Visai*

Cite This: *ACS Omega* 2023, 8, 42264−42274

Read Online

ACCESS | Metrics & More | Article Recommendations | Supporting Information

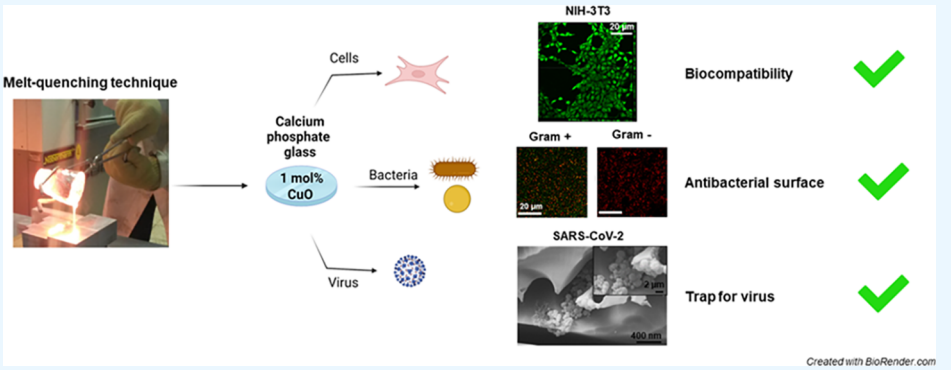

ABSTRACT: Calcium phosphate glasses (CPGs) are acquiring great importance in the biomedical field because of their thermomechanical and bioresorbable properties. In this study, optically transparent copper (1 mol %)-doped calcium phosphate glasses (CPGs_Cu) were prepared through the melt-quenching method, and their biocompatibility and antibacterial and antiviral properties were evaluated and compared with undoped CPGs. Biocompatibility was evaluated on murine fibroblast NIH-3T3 cells as a preliminary study of cytocompatibility. The *in vitro* tests were performed through indirect and direct cytotoxicity analyses by MTT and Alamar Blue assays and supported by electron microscopy observations. Microbiological analyses were performed against the most common Gram-negative and Gram-positive pathogens that cause nosocomial infections: *Escherichia coli*, *Pseudomonas aeruginosa*, *Klebsiella pneumoniae*, *Staphylococcus aureus*, and the methicillin-resistant *Staphylococcus aureus* strain. In addition, the bioglass samples were exposed to SARS-CoV-2 to assess their effects on viral survival. The obtained results assessed the biocompatibility of both bioglass types and their ability to reduce the viral load and trap the virus. In addition, Cu^{2+}-doped bioglass was found to be antibacterial despite its low content (1 mol %) of copper, making this a promising candidate material for biomedical applications, e.g., surgery probes, drug delivery, and photodynamic therapy.

1. INTRODUCTION

The presence of microorganisms on the surface of biomedical devices or on clothing or tools which are used for medical care may be a cause of nosocomial infections.[1] Such infections generally involve different types of bacterial pathogens[2,3] and viruses[4] that expose hospitalized patients to a high risk of pneumonia or osteomyelitis or several kinds of infections which may affect the lower respiratory tract, urinary tract, or bloodstream.[5] The misuse or overuse of antibiotics has, at the same time, itself increased bacterial resistance, constituting a global challenge to the efficacy of antibiotics. In the face of this challenge, there has been considerable research interest in the use of bioresorbable materials with antimicrobial agents for implantable medical devices. Although polymers (e.g., polylactic acid - PLA and poly(lactic-*co*-glycolic) acid - PLGA) have been the most commonly used materials for bioresorbable applications, it is acknowledged that as they degrade and break down, they may generate potentially toxic crystalline fragments within the body.[6] Phosphate-based glasses, on the other hand, are free of this issue and show a high degree of resorbability when compared with other glasses such as silicate and have, in the last decades,[7,8] been increasingly recognized as a promising class of bioactive materials for tissue regeneration applications.[9] Suitable

Received: June 16, 2023
Accepted: October 4, 2023
Published: November 1, 2023

Downloaded via INST NAZIONALE RICERCA METROLOGICA on November 24, 2023 at 09:00:53 (UTC).
See https://pubs.acs.org/sharingguidelines for options on how to legitimately share published articles.

© 2023 The Authors. Published by American Chemical Society

compositions of phosphate-based glasses have also been proven to be optically transparent and are capable of being processed, with different techniques, into microstructured scaffolds, optical fibers, or capillaries.[10−12] This allows for their use in several applications (including *in vivo* sensing, imaging techniques,[11] and photodynamic therapy),[13] thanks to their bioresorbability already proven *in vitro* and *in vivo*.[8,12] Among the different metal ions that have been proposed as antimicrobial agents in biomaterial science,[14,15] the medical value of copper was recognized in antiquity and is acknowledged with the more recent discovery of its role in promoting tissue regrowth and angiogenesis.[9,16] The antibacterial[9,15,17] and virucidal properties[18,19] of copper are due to Cu^{2+} ions that as they enter bacterial cells, they are able to disrupt the membrane causing cytoplasm loss, can degrade the genome and the proteins, and can generate reactive oxygen species (ROS) that cause oxidative stress in cells.[20] The same effect is observed against viruses.[21,22] These properties have been reviewed again in the context research following the COVID-19 pandemic caused by the SARS-CoV-2 virus in 2020, with notable contributions by the National Institute of Health (NIH)[23] and other scientists[21] who have demonstrated that the SARS-CoV-2 virus cannot survive for long periods on copper or copper alloys surfaces[21−25] as reported above. The antibacterial and virucidal efficacy was exerted after contact with a surface/scaffold containing a minimum of 2 mol % of Cu,[18,26,27] and this effect increased with higher amounts of copper.[28] Although interesting research has been published, the antibacterial activity of metal ions and copper in particular has not been explored at concentrations lower than a few percent. The effectiveness of these metal ions, in sufficient high levels of concentration, against microorganisms is clear, but the side effects are significant, damaging the viability of eukaryotic cells.[27] This is a particular concern in the context of this study given that we are proposing to target the antibacterial properties of Cu-doped phosphate glasses in tissue engineering and regenerative medicine. However, as reported above, phosphate glasses can be transparent and be drawn as a fiber optics guiding light, allowing to realize implantable devices for diagnostics and photodynamic therapy.[29,30] This fact can represent a major advance for bioresorbable and implantable fiber optic devices for personalized medicine. The objective of the present study is to synthesize and characterize low-concentration copper-doped glasses (CPGs_Cu) with 1 mol % CuO and undoped glasses (CPGs), starting from a calcium phosphate formulation that is transparent and drawable in fiber forms. One mol % copper was added to avoid altering the transparency but maintaining the antimicrobial properties, although the minimum antimicrobial effect known in the literature was observed using 2 mol % copper.[18,26,27] Subsequently they are biologically analyzed for assessing their biocompatibility and antimicrobial properties against reference infective bacterial strains. Furthermore, they are tested against the SARS-CoV-2 virus.

2. MATERIALS AND METHODS

2.1. Bioglass Synthesis. The undoped and Cu-doped CPGs used in this work (composition (in mol %) $[(50\ P_2O_5 - 25\ CaO - 8\ MgO - 11.5\ Na_2O - 2.5\ B_2O_3 - 3\ SiO_2)x - (CuO)y$, with $x = 1$ when $y = 0$ and $x = 0.99$ when $y = 1]$) were prepared with a conventional melt-quenching technique using high-purity (99+%) biocompatible chemicals as previously reported.[10] The chemicals were weighed and mixed within a dry box to minimize the hydroxyl ion (OH^-) content in the glass. The batched chemicals were melted in a quartz crucible at a temperature of 1200 °C for 1 h under a controlled atmosphere; the melt was cast into a preheated 8 mm diameter steel mold, then annealed at 440 °C for 5 h to relieve internal stresses, and finally cooled slowly to room temperature (RT).

2.2. Bioglass Characterization. The glass density was measured at RT with the Archimedes method using distilled water (dH_2O) as the immersion fluid, with an estimated error of 0.005 g/cm^3. Differential thermal analysis (DTA) was performed using a Netzsch DTA 404 PC Eos differential thermal analyzer at up to 1200 °C with a heating rate of 5 °C/min in sealed Pt/Rh pans to measure the glass transition temperature (T_g) and the onset crystallization temperature (T_x). An error of ±3 °C was observed in the measurement of these characteristic temperatures. X-ray diffraction (XRD) analysis was carried out with an Empyrean Panalytical (Malvern) diffractometer with Cu Kα X-ray radiation (λ = 1.5418 Å) to confirm the amorphous nature of the synthesized glasses. Data were collected in a $\theta-2\theta$ configuration having 2θ values ranging from 10 up to 70° with a step size of 0.01°. The ultraviolet−visible-near-infrared (UV−vis−NIR) transmittance spectra were measured at RT for wavelengths ranging from 200 to 900 nm using a double-beam scanning spectrophotometer (Shimadzu UV-2600, USA) to define the transparency and the UV edge of the glass samples. The thickness of the samples polished with 1 μm diamond paste on both sides was 1.00 ± 0.03 mm. The refractive index (n) was measured at five different wavelengths (633, 855, 1061, 1312, and 1533 nm) through a Metricon 2010 prism coupler. Ten scans were performed for each measurement, and the estimated error of the measurement was ±0.001. The surface roughness of both types of bioglass was measured using a stylus surface profilometer (Intra Touch, Taylor Hobson, UK). The data were processed using ProfilmOnline analysis software. The contact angle was measured with a KSV CAM200 instrument (KSV Instrument Ltd., Finland) with the water sessile drop method.[31] The measurements were acquired with distilled water and cell medium.

2.3. Energy-Dispersive X-ray Spectrometry. High-resolution images of the bioglasses and the map of atomic elements composing the scaffolds were acquired through energy-dispersive X-ray spectrometry (EDS) (Oxford Scientific, OXFORD INCA Energy 350 X-Max 50, UK) and scanning electron microscopy (SEM) (Zeiss, EVO MA10-HR "dual gun", Germany) at 20 kV.

2.4. Ion Release Study. To evaluate the release of the ions, the bioglass samples were immersed in a 6-well plate with 4 mL of double-distilled water (ddH_2O), and the plate was incubated at 37 °C, 5% CO_2. After 3 h, the solution was recovered and acidified with HNO_3. 4 mL were then added, and the procedure was repeated after 6, 9, 24, 48, 72, and 168 h. The obtained solutions were analyzed for the presence of Ca, P, SiO_2, B, Mg, Na, and Cu, considering 4 mL of ddH_2O + 40 μL HNO_3 as the control. Analysis was performed using inductively coupled plasma − optical emission spectroscopy (ICP-OES, Optima 3300 DV PerkinElmer).

2.5. Fibroblast, Bacterial, and Viral Culture's Conditions on Bioglasses. *2.5.1. NIH-3T3 Cells and Culture Conditions.* NIH-3T3 (ATCC CRL-1658), from the mouse embryonic fibroblast cell line, was obtained from the American Type Culture Collection (ATCC, Manassas, VA, USA) and used for biocompatibility studies. Cells were cultured at 37 °C

https://doi.org/10.1021/acsomega.3c04293
ACS Omega 2023, 8, 42264−42274

with 5% CO_2 in Dulbecco's modified Eagle's medium (DMEM) with 4.5 g L^{-1} glucose (Invitrogen), supplemented with 10% bovine calf serum (Sigma-Aldrich, USA) and 1% p/v L-glutamine (Lonza, USA). Cells were routinely trypsinized after confluence and then counted and seeded either in wells or on bioglasses.

2.5.2. Bacterial Strains and Culture Conditions. The microorganisms used in this study were *Escherichia coli* ATCC 25922 (*E. coli*), *Staphylococcus aureus* ATCC 25923 (*S. aureus*), methicillin-resistant *Staphylococcus aureus* (*S. aureus* MRSA), *Pseudomonas aeruginosa* PAO1 (*P. aeruginosa*), and *Klebsiella pneumoniae* (clinical isolate) (*K. pneumoniae*) kindly provided by Roberta Migliavacca (Department of Clinical Surgical, Diagnostic and Pediatric Sciences, University of Pavia, Italy). Bacteria were grown in the appropriate medium overnight and under aerobic conditions at 37 °C using a shaker incubator (VDRL Stirrer 711/CT, Asal Srl, Italy). *E. coli* bacteria were grown in Luria−Bertani (LB) broth (ForMedium, UK), *S. aureus* in brain heart infusion (Sigma-Aldrich, USA), and *P. aeruginosa* and *K. pneumoniae* in Mueller Hinton broth (Sigma-Aldrich, USA).

2.5.3. SARS-CoV-2 Isolation and Titration. The SARS-CoV-2 wild-type European strain was isolated from 200 μL of nasopharyngeal swab seeded on confluent VERO E6 cells [VERO C1008 (Vero 76, cloneE6, Vero E6); ATCC CRL-1586] in a 24-well flat-bottom microplate (COSTAR, Corning Incorporated, Corning, NY, USA) that was decontaminated and incubated at 33 °C with 5% CO_2 for 1 h. After inoculum removal, fresh Minimum Essential Medium (MEM) eagle (Lonza Group Ltd., Basel, Switzerland) was added and supplemented with 1% v/v penicillin, streptomycin, glutamine (Euroclone SpA), and 0.1% v/v trypsin. The sample was observed under an inverted microscope, 10× magnification, every other day until cytopathic effect (CPE) development. CPE was characterized by cell enlargement and syncytia formation. After first isolation, the sample was sequenced[32] and propagated in a VERO E6 25 cm^2 cell culture flask (Corning, NY14831, USA) to increase virus titer and to prepare virus stock for bioglass testing. The titer of SARS-CoV-2 was measured as 50% of the tissue culture infectious dose (TCID50) in six replicas in a 96-well flat-bottom tissue-culture microtiter plate. 10-fold serial dilutions from 10^{-1} to 10^{-8} of the virus, in the presence of 3×10^4 VERO E6, were incubated for 72 h at 33 °C in 5% CO_2. The cells were observed under a microscope for CPE appearance and stained with Gram's crystal violet solution (Merck KGaA, Darmstadt, Germany) plus 5% v/v formaldehyde and 40% m/v formaldehyde (Carlo Erba SpA, Arese, Italy). The value of TCID50 mL^{-1} was calculated with the Reed−Muench method.[33]

2.6. Viability Assays. *2.6.1. NIH-3T3 Cell Viability Assays.* A drop of cell suspension was added on top of the scaffolds, and after 20 min, 0.4 mL of culture medium was added to cover the sterile scaffolds. After the desired incubation time, cell viability, morphology and quantitative extracellular protein expression were evaluated.[34] Cell viability was evaluated through indirect and direct contact experiments.

2.6.1.1. Cell Viability by Indirect Contact. DMEM was incubated at 37 °C and 5% CO_2 on bioglasses for 24 and 48 h to evaluate if the scaffolds released cytotoxic compounds. At the end of the incubation time, 2-fold serial dilutions of overnight solutions were performed in a 96-well plate and incubated with NIH-3T3 cells (2×10^4/well) for 24 h at 37 °C + 5% CO_2. After incubation, the cells were washed with sterile phosphate-buffered saline (PBS) 1× and incubated with a base medium supplemented by 10% of 3-(4,5-dimethylthiazole-2-yl)-2,5-diphenyl tetrazolium bromide (MTT) (Sigma-Aldrich, USA) for 3 h at 37 °C + 5% CO_2. The reaction was blocked as described[14] and analyzed with a CLARIOstar (BMG Labtech, Germany) plate reader at 595 nm wavelength with the reference wavelength of 655 nm. Titration curve interpolation was used to express the number of cells in each sample. The results were normalized to a tissue culture plate (TCP) which was used as a control, represented by cells grown in a medium.

2.6.1.2. Cell Viability by Direct Contact. 5×10^4 cells/well were seeded on bioglasses. Viability was evaluated with Alamar Blue, a resazurin-based assay (TOX8−1KT Sigma-Aldrich, USA), after 24, 48, 72, and 168 h. Briefly, at each time point, the culture medium was replaced by the same volume of fresh medium with 10% Alamar Blue.[35,36] The absorbance was read with a CLARIOstar (BMG Labtech, Germany) plate reader at 600 nm with 690 nm as the reference wavelength.[37,38] Titration curve interpolation was used to express the number of cells for each sample.

2.6.2. Bacterial Viability Assays. 200 μL of 1×10^5 bacteria were incubated for 24 h at 37 °C on CPG, CPG_Cu bioglasses, and in TCP wells. Two analyses of bacterial viability were performed through MTT:[14] on the supernatant previously removed from the scaffolds (*analysis 1*) and on the bacteria adherent to the scaffold's surfaces (*analysis 2*). *Analysis 1*: the supernatant, composed of planktonic bacteria, was transferred into another TCP well and incubated with 10% of MTT. *Analysis 2*: after the removal of planktonic bacteria, the scaffolds were washed with PBS 1× and transferred into another TCP well. 200 μL of PBS 1× was added with 10% of MTT, and the viability was determined as previously described. Results were normalized to the TCP used as the control, represented by bacteria grown in the medium.

2.6.3. SARS-CoV-2 Viability Assays. The biomaterials were placed in a 36-well plate, covered with 300 μL of SARS-CoV-2 (B.1, D614G) at 10^4 TCID50, and incubated at 33 °C + 5% CO_2 for 1 or 4 h. At the same time, 300 μL of virus at 10^4 TCID50 was dispensed on confocal glasses as the control. After incubation, viral activity was assessed through titration on VERO E6 cells as previously described. The samples were washed three times with trypsin EDTA 1× to remove the viral particles attached to their surfaces. The viral activity after washing was assessed, as before, by titration on VERO E6. Each experiment was performed in triplicate.

2.7. Enzyme-Linked Immunosorbent Assay on NIH-3T3 Cells. 5×10^4 cells/samples were seeded on scaffolds. After 7 days, the scaffolds were gently washed with PBS 1× and incubated on ice for 20 min with 300 μL of a solution containing a radio-immunoprecipitation assay 1× lysis buffer, 1 mM sodium orthovanadate, and 1 mM protease inhibitor (Sigma-Aldrich, USA).[39] The detached cells were then sonicated for 5 min at RT and centrifuged for 10 min at 15,000 rpm, at 4 °C.[40] The total protein concentration was evaluated with a bicinchoninic acid protein assay kit (Pierce Biotechnology, Inc., USA) according to the manufacturer's instructions. To measure the produced extracellular matrix (ECM) collagen type I and fibronectin, an enzyme-linked immunosorbent assay (ELISA) was performed on the extracted ECM proteins as described by Saino et al.[41] The absorbances of each sample were plotted against a calibration curve containing known amounts of each protein. The amount

https://doi.org/10.1021/acsomega.3c04293
ACS Omega 2023, 8, 42264−42274

of ECM constituents in the different samples was expressed as μg/scaffold.

2.8. Confocal Laser Scanning Microscopy Studies. *2.8.1. NIH-3T3 and Bacterial Cell Viability.* NIH-3T3 were incubated on scaffolds for 48 h and bacteria for 24 h, as previously described. Both eukaryotic and prokaryotic adherent cells were evaluated with the LIVE/DEAD BacLight viability kit (Molecular Probes, USA) as reported by Sprio et al.[14] The cells were observed using confocal laser scanning microscopy (CLSM) (Leica, model TCS SP8 DLS, Leica, Germany). NIH-3T3 cells were observed using a 20 and 40× objective, whereas bacteria were observed using a 63× oil immersion objective. Three-dimensional (3D) projections of NIH-3T3 cells were obtained using the software LAS X (Leica Microsystems, Wetzlar, Germany).

2.8.2. NIH-3T3 Cell Morphology. 7×10^4 cells/samples were seeded on the bioglasses and incubated for 24 h at 37 °C + 5% CO_2. After the removal of the medium and PBS 1× washes, the cells were fixed and treated as described.[35,39] After PBS washes and coating with BSA 1% for 1 h at RT, the cytoskeletal β-tubulin was stained with an Alexa-Fluor 488 anti-β-tubulin antibody (1:25 dilution) (Sigma-Aldrich, USA) for 1 h at RT. Nuclei were stained with 2 μg/mL Hoechst 33342 (Sigma-Aldrich, USA) for 10 min at RT.[42] At the end of incubation, the scaffolds were washed in PBS 1×, and images were taken at 20 and 63× magnifications.

2.9. Scanning Electron Microscopy Observations. Cells and viruses were incubated on the scaffolds, and then the samples were washed with PBS 1× and treated as described.[35,43] Fibroblasts images were acquired at 1 and 3 k× magnifications. Bacterial images were acquired at 5 and 10 k× and SARS-CoV-2 at 25 and 80 k×.

2.10. Statistical Analysis. All statistical calculations were carried out by considering the mean of the results (in triplicate) obtained from two separate experiments. The analysis was carried out using GraphPad Prism 9 (GraphPad Inc., USA). Statistical analysis was performed using Student's unpaired, two-sided t test (significance level of $p < 0.05$) with respect to TCP control. Two-way analysis of variance, followed by Bonferroni's multiple comparisons test, was also performed.[43]

3. RESULTS

3.1. Characterization of Bioglasses and Ion Release Analysis. The scaffolds used in this work were CPG and CPG_Cu (Figure 1A,B). The macroscopic images were acquired from the authors. The bioglasses microstructure (Figure 1C,D) was investigated by SEM.

The XRD analysis of the bioglasses is reported in Supplementary Figure S1. Both CPG glasses present the characteristic shape of an amorphous glass. Compositional analysis carried out using an Inca Oxford Instrument (EDS) allowed mapping (Supplementary Figure S2A,B) of the relative position of Ca, P, Mg, Na, Si, and Cu on the surface of (A) CPG and (B) CPG_Cu and determination of their percentages, as shown in Supplementary Figure S2ii-iii. Unfortunately, copper was not detected in the CPG_Cu sample because of the very low concentration level. Within the experimental error, EDS analysis showed that the quantity of the elements (Supporting Information Figure S2iii) was quite similar in both bioglass samples and that their distribution on the surfaces of bioglasses is homogeneous. The surface roughnesses of both samples showed comparable surface roughness values of 1.21 and 1.73 μm, respectively. Table 1 reports the thermal properties and density of the undoped and Cu^{2+}-doped CPGs, while the DTA thermogram of the Cu^{2+}-doped CPG is shown in Supporting Information Figure S3.

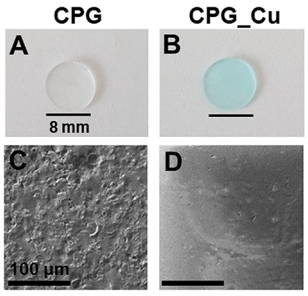

Figure 1. CPG macroscopic and microscopic images. (A, B) Macroscopic images of (A) undoped CPG and (B) CPG_Cu were acquired by the authors. Bioglass dimensions: 8 mm diameter and 0.9 mm thickness. (C, D) Microscopic images of (C) CPG and (D) CPG_Cu surfaces obtained through SEM at 1 k× magnification (100 μm bar).

The transmittance (T%) spectra of the undoped and Cu^{2+}-doped CPGs in the wavelength range of 200−900 nm are shown in Figure 2A. Panel B of Figure 2 shows the dependence of the refractive index on the incident wavelength in the absence or in the presence of Cu^{2+} ion doping.

The CPG and CPG_Cu glass samples were immersed in ddH_2O to measure the release of different elements through ICP-OES at different times (3, 6, 9, 24, 48, 72, and 168 h). To emphasize the results, Figure 3 shows the release rate of the different samples, i.e., the amount of each released element normalized with time. In this way, it is possible to see that after a settling time of about 24 h, the release rate of all of the elements becomes nearly constant.

The CPG and CPG_Cu samples were immersed in ddH_2O for several days, and the concentration of different elements was measured at regular times. Supplementary Table S1 reports only the initial and the released quantities after 168 h. In addition, to determine the wettability of bioglass surfaces, the contact angle was measured not only with ddH_2O but also with a eukaryotic cell medium. The values reported in Supporting Information Table S2 demonstrate that both surfaces are hydrophilic, particularly CPGs. The obtained results show that the contact angle of surfaces decreased[44] to a greater extent with the cellular medium when compared with water. This indicates a major hydrophilicity and thus a high wettability of the surfaces.

3.2. Evaluation of NIH-3T3 Fibroblast Viability and Morphology. The biocompatibility of bioglasses was evaluated by investigating the viability of NIH-3T3 cells derived from mouse embryonic fibroblast cell lines. First, the content released from CPG and CPG_Cu was diluted, and the viability of NIH-3T3 cells was evaluated through an indirect contact cytotoxicity experiment after 24 and 48 h. The results reported in Figure S4 show that neither of the bioglasses released any toxic substances. Furthermore, the evaluation of cell viability and morphology (Figure 4) on the bioglasses was performed by direct contact.

NIH-3T3 cells were seeded onto bioglasses, and their viability (Figure 4A) was evaluated at different incubation times using Alamar Blue.[26] The viability was represented as folding increase, i.e., the number of viable cells grown at 24, 48, 72, and 168 h compared to the number of seeded cells. Figure

https://doi.org/10.1021/acsomega.3c04293
ACS Omega 2023, 8, 42264−42274

Table 1. Thermal and Physical Properties of CPG and CPG_Cu

glass name	$T_g \pm 3$ (°C)[a]	$T_x \pm 3$ (°C)[b]	$\Delta T = T_x - T_g \pm 6$ (°C)[c]	$\rho \pm 0.05$ (g/cm^3)[d]
CPG	438	631	193	2.60
CPG_Cu	456	670	214	2.61

[a]Glass transition temperature T_g. [b]Onset crystallization temperature T_x. [c]Glass stability parameter ΔT. [d]Density ρ.

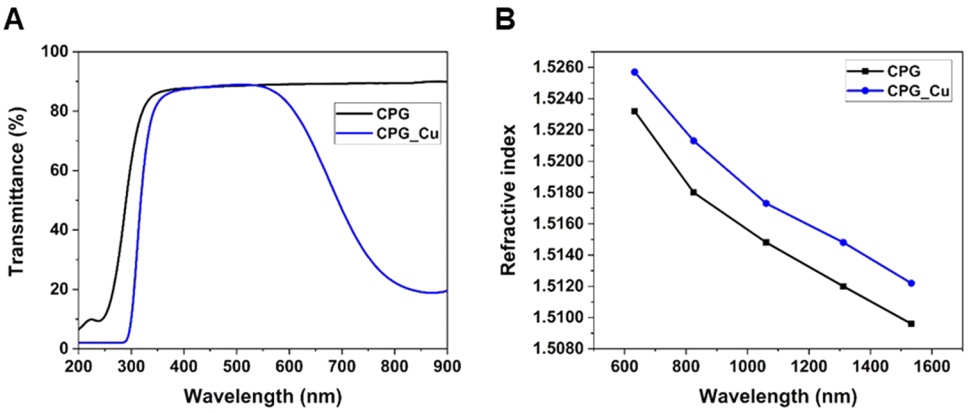

Figure 2. Optical properties. (A) UV−vis−NIR transmittance spectra and (B) refractive index values of undoped and Cu^{2+}-doped CPGs as a function of the wavelength.

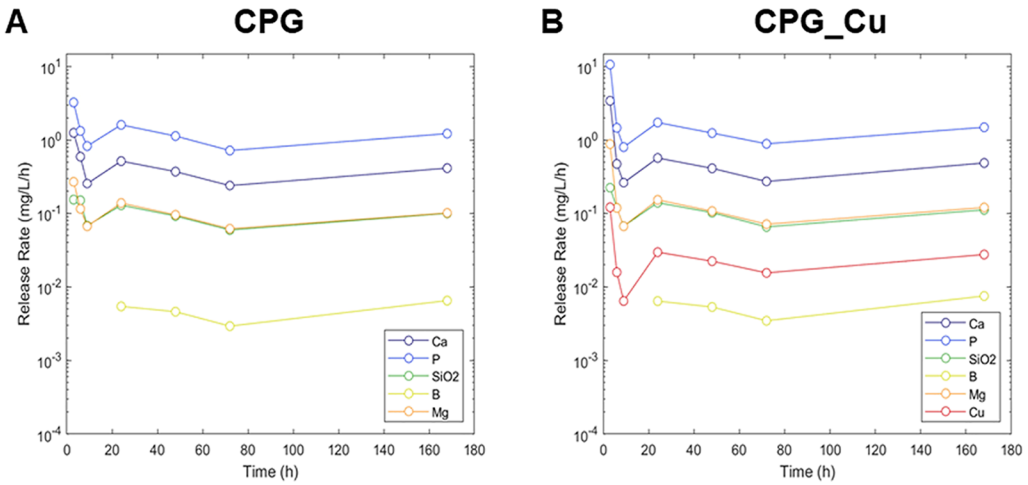

Figure 3. Elements release. Rate of release of different elements against time (3, 6, 9, 24, 48, 72, and 168 h) upon immersion in ddH_2O. (A) Samples without Cu; (B) samples with Cu.

4A shows that cells exponentially grew over time on both types of bioglass, demonstrating that the addition of copper did not reduce the adhesion and growth of cells. In addition, quantitative cell viability data were supported by CLSM analyses (Figure 4B) which showed viable cells after 48 h of growth on the bioglasses, as already reported in the literature.[26,45] Moreover, Figure 4C also shows the biocompatibility of the scaffolds. It is possible to notice that after 24 h of adhesion, cells had a classic fibroblast shape due to the cytoskeleton marked in green and well-formed nuclei in blue. SEM images in Figure 4D acquired after 7 days of cell incubation on scaffolds demonstrate a well-formed layer of cells. To evaluate the amount of ECM components from fibroblasts grown on CPG and CPG_Cu bioglasses, proteins such as collagen type I and fibronectin were extracted after 7 days and quantified (Table 2).

The results showed a higher deposition of the ECM on CPG than on CPG_Cu. This is supported by hydrophilicity shown by both surfaces, reporting a contact angle (Supporting Information Table S2) of CPG lower than that of CPG_Cu, ca. 12.0° and ca. 22.5°, respectively.

3.3. Evaluation of Antibacterial Activity. Bacterial viability was evaluated through MTT on planktonic cultures represented by bacteria floating in the medium incubated on bioglasses (planktonic supernatant) and bacteria that adhered on the surfaces. Figure 5 shows the viability of bacterial supernatant (*analysis 1*) − composed of planktonic bacteria, which was in contact with the bioglasses. This analysis is important to determine whether copper and other ions released from the bioglasses have an antibacterial effect. From the data, it is possible to notice that Gram-positive bacteria (Figure 5A) were alive after 24 h of contact with both CPG and CPG_Cu samples, suggesting that the ions released from the scaffolds were not able to kill the bacteria. However, the interesting result was that the addition of a low quantity of copper (1 mol %) was sufficient to significantly reduce, by about 60 and 80%, the viability of Gram-negative bacteria (Figure 5B) with respect to CPG. Statistical analyses were

https://doi.org/10.1021/acsomega.3c04293
ACS Omega 2023, 8, 42264−42274

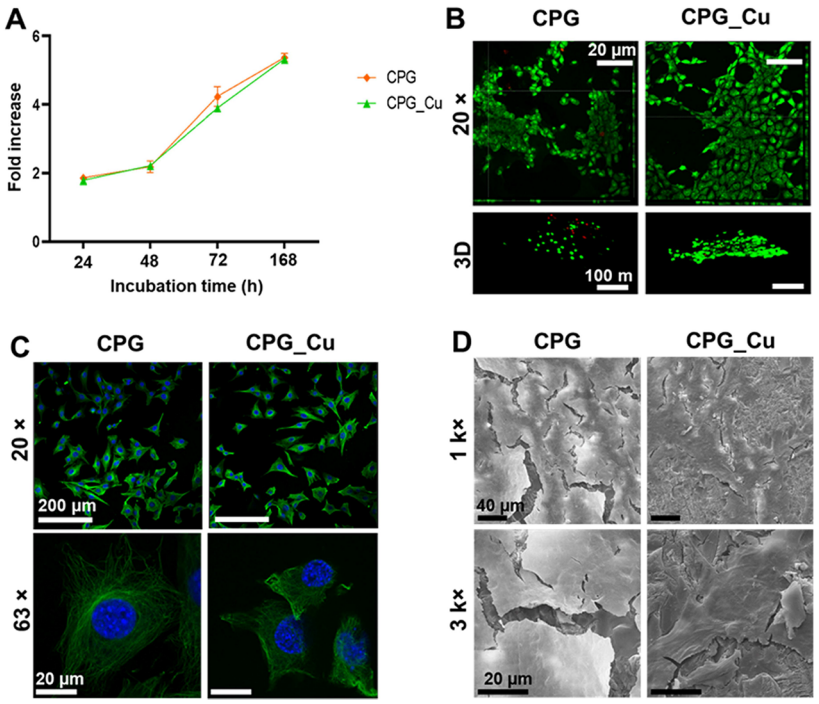

Figure 4. NIH-3T3 adherence and viability on bioglasses. NIH-3T3 fibroblasts were seeded on the scaffolds. (A) Viability was tested with Alamar Blue assay after 24, 48, 72, and 168 h and was expressed as fold increase with respect to the number of seeded cells. (B) CLSM analysis of cells on CPG and CPG_Cu after 48 h of adhesion. Live cells (green) were stained with Syto 9 dye, whereas dead cells (red) were stained with propidium iodide. Orthogonal projections of NIH-3T3 cells at 20× , scale bars (see CPG) = 20 μm. 3D projections at 40× , scale bars (see CPG) = 100 m. (C) Morphology of cells. After 24 h of adhesion, nuclei were stained with Hoechst 33342 (blue) and cytoskeletal β-tubulin with an antibody anti-β-tubulin (green). Distribution of cells on the surface at 20× , scale bar (see CPG) = 200 μm. Fibroblasts magnified images at 63× (electron zoom 2.5), scale bar (see CPG) = 20 μm. (D) SEM images acquired after 7 days of growth on bioglasses. Images acquired at 1 k× magnification, scale bars (see CPG) = 40 μm and 3 k× (scale bars = 20 μm).

Table 2. Quantification of Collagen and Fibronectin Deposited on Bioglass

scaffold[a]	collagen I (μg/scaffold)[b]	fibronectin (μg/scaffold)[b]
CPG	2.55 ± 0.05	0.49 ± 0.03
CPG_Cu	1.93 ± 0.06	0.38 ± 0.02

[a]NIH-3T3 were seeded on the scaffolds. After 7 days, collagen type I and fibronectin contents were extracted and quantified through an ELISA assay. [b]Data report extracellular matrix proteins as μg ± SD.

performed in comparison to the TCP control, represented by bacteria grown in the medium in the well and set as 100% of bacterial viability (red line).

After the removal of planktonic cultures from bioglasses, the viability was assessed on bacteria remaining adherent on surfaces (*analysis 2*) (Figure 6A,B). This analysis is relevant to evaluate if the surface itself retains antiadhesive properties. Viable and dead bacteria were observed by CLSM (Figure

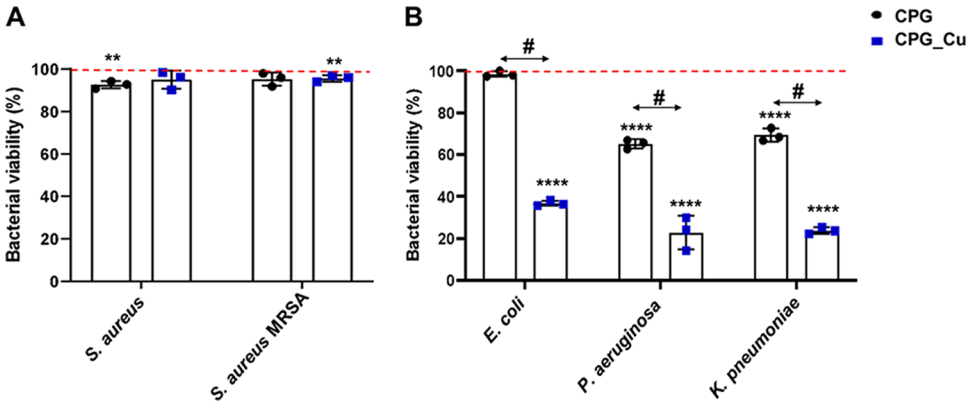

Figure 5. Bacterial viability of planktonic cultures seeded on bioglasses. (A) Gram-positive and (B) Gram-negative bacteria were incubated through direct contact with scaffolds for 24 h at 37 °C. The viability of bacteria was assessed with MTT as described in the Materials and Methods section. The supernatant composed of planktonic bacteria was transferred to another well and evaluated with MTT. The data were represented as percentage of bacterial viability with respect to the TCP control, represented by bacteria grown in LB medium and set as 100% (red line). Error bars indicate the standard deviation (SD) of the mean values of the replicates (n = 3). *, # Statistical analysis. (*) represents the analysis with respect to TCP: p value <0.01 (**); p < 0.0001 (****). Multiple comparison between CPG and CPG_Cu (#) was performed (p < 0.0001).

https://doi.org/10.1021/acsomega.3c04293
ACS Omega 2023, 8, 42264−42274

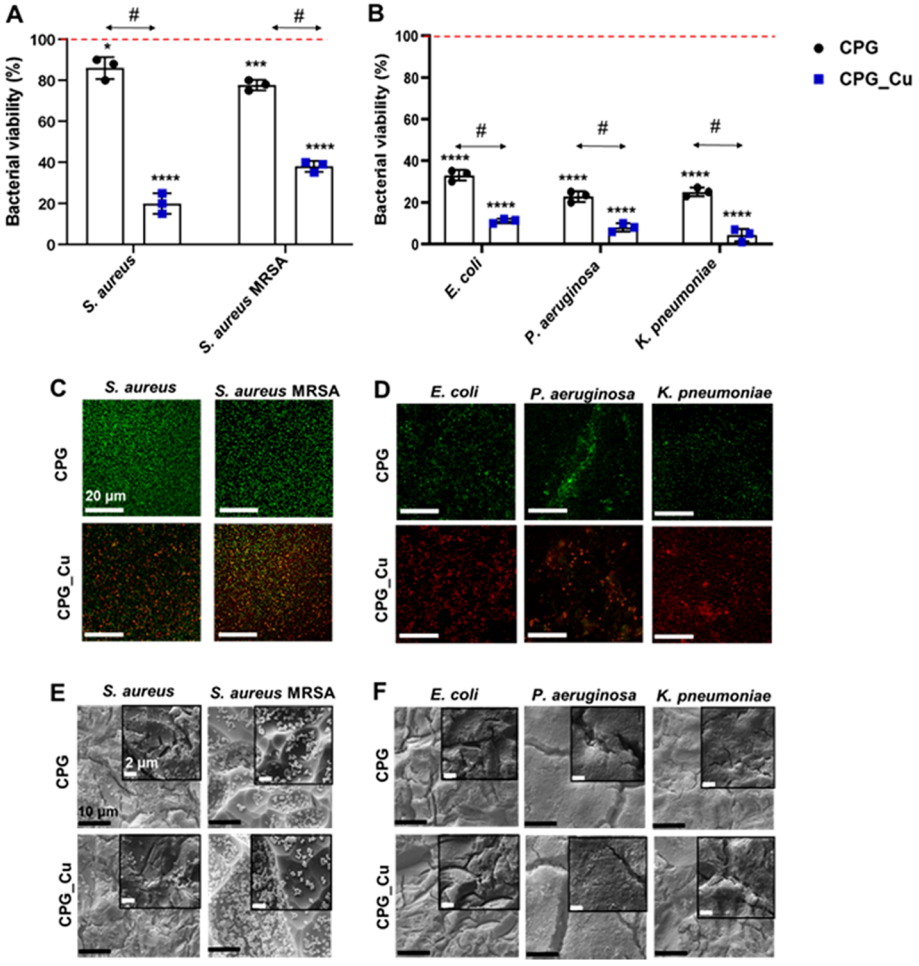

Figure 6. Bacterial adhesion on bioglasses. (A–E) Gram-positive and (B–F) Gram-negative bacteria were incubated through direct contact with scaffolds for 24 h at 37 °C. (A–D) After the removal of planktonic bacteria, the viability of attached cells was evaluated. (A, B) Viability was assessed with MTT as described inSection 2. The data were represented as percentage of bacterial viability with respect to the TCP control, represented by bacteria that adhered in the well and set as 100% (red line). Error bars indicate the SD of the mean values of the replicates (n = 3). *, # Statistical analysis. (*) represents the analysis with respect to TCP: p value <0.05 (*), $p < 0.001$ (***), and $p < 0.0001$ (****). Multiple comparison between CPG and CPG_Cu (#) was performed ($p < 0.0001$). (C, D) CLSM analyses of (C) Gram-positive and (D) Gram-negative bacteria on bioglass scaffolds showed live cells (green) stained with Syto 9 dye and dead cells (red) stained with propidium iodide. All images were acquired at 63×. Scale bars (see *S. aureus*, C panel) = 20 μm. (E, F) SEM images of (E) Gram-positive and (F) Gram-negative bacteria were acquired for all bacteria at 5 k× magnification, insets 10 k×. Scale bars (see E) = 10 μm; insets: 2 μm.

6C,D). In addition, bacterial distribution (Figure 6E,F) on surfaces was acquired with SEM. Panels A and B of Figure 6 show that undoped CPG surfaces killed ca. 20% of *S. aureus* and MRSA strain (Figure 6A). The viability of Gram-negative bacteria (Figure 6B), on the other hand, was significantly reduced by 70–80%, with respect to the TCP control (red line). The presence of 1 mol % copper in CPG_Cu, however, reduced the viability of adherent *S. aureus* and MRSA strains (Figure 6A) by ca. 80 and 60%, respectively. In addition, the CPG_Cu surfaces significantly reduced the viability of adherent Gram-negative bacteria (Figure 6B). In particular, the *E. coli* viability was reduced by 90%, whereas those of *P. aeruginosa* and *K. pneumoniae* were reduced by ca. 95%. The results were confirmed by CLSM images (Figure 6C,D). Panels E and F of Figure 6 show SEM images of bacterial adhesion on bioglasses. The images acquired on the glass control are in Supporting Information Figure S5. In the SEM image, the presence of bacteria is noted, but it is evident that some of them were located inside clefts and could not be detected by the instrument (Figure 6F).

3.4. Evaluation of Bioglass Effect against SARS-CoV-2. The impact of bioglasses on SARS-CoV-2 survival and their capacity to act as molecular traps for viral particles, was evaluated. The SARS-CoV-2 strain (B.1, D614G) was incubated on CPG, CPG_Cu, and on a confocal glass (as a control) for 1 and 4 h at 33 °C + 5% CO_2. After incubation, the inoculum was titrated on VERO E6 (*pre-treatment*). The samples were washed with trypsin to detach the trapped viral particles (*post-treatment*), and SARS-CoV-2 titer was determined (Figure S6). The results are reported in Table 3 with the percentage of virus retained on the bioglass samples.

For both times assayed (1 and 4 h), the CPG bioglass samples retained the higher concentration of SARS-CoV-2. The longer the exposure time, the greater the concentration of retained viral particles on the surface. The control glass did not have any sticky surface characteristics and thus was not able to retain SARS-CoV-2. Moreover, SEM images (Figure 7) of viruses on the bioglasses were acquired after 1 and 4 h.

https://doi.org/10.1021/acsomega.3c04293
ACS Omega 2023, 8, 42264–42274

Table 3. Titration of SARS-CoV-2 on Bioglasses

time of exposition	sample	viral titer (TCID50 mL^{-1})[a] pre-treatment	viral titer (TCID50 mL^{-1})[a] post-treatment	retained virus (%)
1 h	Glass	422	5	1.18
	CPG	208	56	26.92
	CPG_Cu	396	23	5.81
4 h	Glass	215	9	4.19
	CPG	198	104	52.53
	CPG_Cu	196	45	22.96

[a]SARS-CoV-2 was incubated for 1 and 4 h onto CPG, CPG_Cu, and a control confocal glass. After the incubation time, the inoculum was titrated on VERO E6 (*pre-treatment*); then the glasses were washed with trypsin (*post-treatment*) and titrated to assess the percentage of viable SARS-CoV-2 retained on bioglasses.

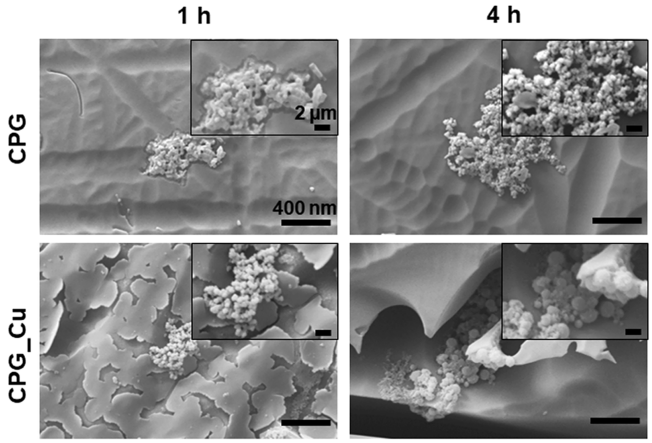

Figure 7. SEM images of SARS-CoV-2. Virus on bioglasses in pre-treatment condition after 1 and 4 h of incubation. All images acquired at 25 k× magnification, insets at 80 k×. Scale bar (see CPG) = 400 nm; insets 2 μm.

4. DISCUSSION

In this study, optically transparent CPGs were synthesized through the traditional melt-quenching method and produced with and without 1 mol % of CuO (CPGs_Cu) which was added to confer antimicrobial properties but in a concentration that would not affect glass transparency. The morphological, physical, thermal, optical, and biological properties of both types of bioglasses were thoroughly analyzed. Biological analyses were performed to investigate their cytocompatibility and antimicrobial activity. In terms of thermal properties, the Cu^{2+}-doped CPG exhibited higher T_g and T_x than the undoped CPG. A glass stability parameter of around $\Delta T = 200 \pm 6$ °C for both glasses suggests that they are stable against devitrification and suitable for crystal-free fiber drawing. It was also demonstrated that the addition of Cu^{2+} ions did not negatively impact CPG density. Moreover, both the CPG and CPG_Cu formulations showed a *T*% value of around 90% in the wavelength ranges of ca. 350−900 and 400−540 nm, respectively. After 540 nm, the transmittance of the CPG_Cu experienced a rapid decrease with a final value of 20% at 900 nm. Moreover, the doping of the CPG with 1 mol % CuO led to a red shift in the UV absorption edge of around 30 nm. Interestingly, the addition of Cu^{2+} metal ions led to an increase in the refractive index values of CPG at all wavelengths. Copper is an important element and is essential for many enzymes and important cofactors of the human body.[18,46] Notwithstanding the acknowledged usefulness of copper for cells,[47] it is necessary to strictly control quantities, either to introduce or release, as high doses of Cu^{2+} ions increase ROS production and consequently decreases cell viability.[9,26,48,49] A fibroblast cell line was used to assess bioglass cytocompatibility. The obtained results confirmed the cytocompatibility of both scaffolds: both formulations presented a roughness lower than 2 μm and possessed sufficient levels of surface hydrophilicity and, as such, were demonstrated to support the adhesion and growth of eukaryotic cells.[31,44] Indeed, it is known in the literature that a high level of hydrophilicity allows the adhesion of both prokaryotic and eukaryotic cells to surfaces.[44,50] Eukaryotic cells when adhered on scaffolds could spread on the surface by depositing ECM proteins,[44,49,50] thanks to the prehydration of surfaces that ameliorate the initial chance for cells to adhere on surfaces.[44] It is important to highlight that the status, instead of the number of deposited ECM proteins, can be important in cell adhesion on surfaces[44] because when the proteins are adsorbed by hydrophobic surfaces, they are in a denatured state and their geometry does not allow them to promote cell adhesion.[44,49,50] It is notable that the presence of copper ions did not decrease cell adhesion and growth. This ion is reported in the literature[48] to be involved in promoting cell differentiation, osteogenic-related gene expression, and also ECM protein deposition such as fibronectin and collagen type I.[48−50] To assess the impact of the addition of the broad-spectrum antimicrobial copper ion, the bioglasses were tested against five of the most infective bacterial pathogens and against the SARS-CoV-2 virus. This was to evaluate whether the presence of a very low concentration of copper (1 mol %) would be effective, given that the current agreed position in the literature is that the minimum concentration required for antibacterial and virucidal activities is 2 mol %.[18,26,27] The analyses were performed on planktonic cultures removed from the scaffolds and on planktonic bacteria that remained attached to the surface. The results, interestingly, demonstrated that the presence of only 1 mol % copper was in fact sufficient to generate an antibacterial effect in the CPG_Cu bioglass. Copper was more effective against Gram-negative than Gram-positive bacteria as already reported in the literature,[18,26,51] with the variations in effectiveness against different bacterial strains being due to differences in the cell wall structure.[52] Gram-negative bacteria are characterized by thin cell wall peptidoglycan levels and by the presence of an outer membrane, whereas Gram-positive bacteria present negative teichoic and lipoteichoic acids on the surface that attract positively charged particles.[9,52] Copper-doped bioglass surfaces are more effective against bacteria that are attached on the surfaces because the ions released from the surfaces are easily attracted from adherent bacterial cells. The ions enter and damage the cell, disrupt the cell membrane, and induce the loss of cytoplasmic content, degradation of the genome and generation of ROS which cause oxidative stress.[3,18] It is known, however, that bacteria are able to resist the toxic effect of copper through mechanisms such as the impermeability of their outer and inner membranes to copper ions, the active extrusion mechanism of copper from the cell, and the extracellular sequestration of copper.[28] These resistance mechanisms, along with the low concentration of Cu^{2+} ions (1 mol %), could explain why the CPG_Cu formulation was less effective against *S. aureus* and MRSA bacteria. The low concentration of Cu^{2+} ions released may also

https://doi.org/10.1021/acsomega.3c04293
ACS Omega 2023, 8, 42264−42274

explain the inability of CPG_Cu to neutralize SARS-CoV-2 (data not shown). This is in accordance with what was observed in a recent study where the authors demonstrated that a higher delamination and dissolution of the CuO coating enhances the virucidal effect against human coronavirus 229E.[53] However, even though the levels of Cu^{2+} released were not high enough to have a complete neutralizing effect, the surface structures of these bioglasses were able to act as a trap for SARS-CoV-2 viral particles. Indeed, an indented, porous surface provides a greater area compared to a same size smooth surface. A higher area leads to a faster drying of liquid and niches in which the virus can be retained.[25] Both the drying and trapping of viral particles can reduce the possible transmission of a viable virus. The undoped CPGs were observed to retain high levels of virions on their surface in a time-dependent manner, leading to a reduced viral load in the medium. This trapping effect, observed in both types of bioglass, was due to the electrostatic interactions between the virus and phosphate glasses, and the effect increases with time. The charge of SARS-CoV-2, as is well-known, is not homogeneous: the spike proteins are positively charged[54] and the lower parts are negatively charged.[55,56]

Our results demonstrated that the virions are highly attracted to the negatively charged surface of CPGs: this allows them to act as a trap for viruses, and the effect only increases with time. The lower levels of ability for copper-doped CPGs to attract viruses, when compared with undoped formulations, can be explained by the fact that positively charged copper ions (Cu^{2+}) which may be present on the surface serve to repel SARS-CoV-2 spike proteins. Implementing the release of Cu^{2+} ions, in association with the ability of these bioglasses to rapidly act as traps for viral particles, may further reduce SARS-CoV-2 survival and dissemination rates further. Bioglasses have been found useful in a plethora of different applications, such as soft and bone tissue engineering, as nanoparticles for drug delivery and even in dentistry.[57] Once their virucidal activity is fully implemented, these bioglasses could be used to directly target SARS-CoV-2 by trapping virions onto their surfaces and releasing the correct levels of ions, successfully neutralizing the virus. They could also be used as a protective measure by coating communal surfaces, such as door handles, effectively reducing the pathogen transmission between subsequent users. Our results demonstrate that the presence of copper does not impact the growth of eukaryotic cells in both indirect and direct cytotoxicity analyses and confirm, for the first time, that the presence of very low copper concentrations is in fact sufficient to generate an antibacterial effect. Our final, significant, finding is that these bioglasses are able to trap SARS-CoV-2 on their surfaces, potentially arresting or impeding transmission through the body.

5. CONCLUSIONS

The aim of this study was to investigate the thermomechanical properties of an optically transparent biodegradable glass and to assess the biocompatibility and antibacterial properties, resulting from the presence of 1 mol % CuO concentration, as well as the effect against SARS-CoV-2. Optically transparent, thermally stable glasses were successfully prepared by conventional melt-quenching method and characterized. All samples were demonstrated to be cytocompatible, and the CPG_Cu sample was shown to be effective against bacteria, although the concentration of copper was only at 1 mol %. It is also notable that both bioglass surfaces functioned as a trap for SARS-CoV-2, effectively decreasing the viral survival. Exploring the geometry of the substrates was out of the scope of the present work, although optimized microstructures in the form of fibers or planar substrates are a very promising research direction to explore, possibly leading to a potential improvement in all effects here described. Based on these results, CPG_Cu is not only an interesting material for scaffolds for tissue engineering, regenerative medicine, photodynamic therapy, and drug delivery but also something that could be used in medical applications as surgical probes or coatings for medical devices because of its biocompatibility and efficacy against bacteria.

■ ASSOCIATED CONTENT

Supporting Information

The Supporting Information is available free of charge at https://pubs.acs.org/doi/10.1021/acsomega.3c04293.

XRD spectra of the undoped and Cu^{2+}-doped CPGs; initial and released quantities of different elements after a soaking time of 168 h in ddH_2O measured on the CPG and CPG_Cu samples using ICP-OES; values of contact angle using two different solutions: dH_2O and eukaryotic cell medium; EDS results; maps of elements in CPG and CPG_Cu, 100 μm bar; quantitative results; DTA thermogram of Cu^{2+}-doped CPG; effect of bioglasses released contents on NIH-3T3 cell viability; bacterial adhesion onto coverslips; and SARS-CoV-2 trapping onto biomaterial scaffolds (PDF)

■ AUTHOR INFORMATION

Corresponding Authors

Davide Janner − *Department of Applied Science and Technology, UdR INSTM, Politecnico di Torino, Torino 10129, Italy*; Email: davide.janner@polito.it

Daniel Milanese − *Department of Engineering and Architecture, UdR INSTM, University of Parma, Parma 43121, Italy*; Email: daniel.milanese@unipr.it

Livia Visai − *Department of Molecular Medicine, Center for Health Technologies, UdR INSTM, University of Pavia, Pavia 27100, Italy; Medicina Clinica-Specialistica, UOR5 Laboratorio di Nanotecnologie, ICS Maugeri, IRCCS, Pavia 27100, Italy*; orcid.org/0000-0003-1181-3632; Email: livia.visai@unipv.it

Authors

Elisa Restivo − *Department of Molecular Medicine, Center for Health Technologies, UdR INSTM, University of Pavia, Pavia 27100, Italy*; orcid.org/0000-0003-1752-9341

Diego Pugliese − *Department of Applied Science and Technology, UdR INSTM, Politecnico di Torino, Torino 10129, Italy*; orcid.org/0000-0002-6431-1655

Duccio Gallichi-Nottiani − *Department of Engineering and Architecture, UdR INSTM, University of Parma, Parma 43121, Italy*; orcid.org/0000-0003-1656-5850

José Camilla Sammartino − *Department of Clinical, Surgical, Diagnostic and Pediatric Sciences, University of Pavia, Pavia 27100, Italy*; orcid.org/0000-0003-3707-3118

Nora Bloise − *Department of Molecular Medicine, Center for Health Technologies, UdR INSTM, University of Pavia, Pavia 27100, Italy; Medicina Clinica-Specialistica, UOR5 Laboratorio di Nanotecnologie, ICS Maugeri, IRCCS, Pavia 27100, Italy*; orcid.org/0000-0002-6000-5036

https://doi.org/10.1021/acsomega.3c04293
ACS Omega 2023, 8, 42264−42274

Emanuela Peluso − *Department of Molecular Medicine, Center for Health Technologies, UdR INSTM, University of Pavia, Pavia 27100, Italy;* orcid.org/0009-0009-2882-1613

Elena Percivalle − *Molecular Virology Unit, Microbiology and Virology Department, Fondazione IRCCS Policlinico San Matteo, Pavia 27100, Italy*

Complete contact information is available at: https://pubs.acs.org/10.1021/acsomega.3c04293

Author Contributions

E.R.: conceptualization, investigation, formal analysis, validation, and writing—original draft and editing. D.P.: investigation, formal analysis, validation, and review and editing. D.G.-N.: investigation, formal analysis, validation, and review and editing. J.C.S.: investigation, formal analysis, and review and editing. N.B.: investigation, formal analysis, review and editing. E.P.: investigation. E.P.: investigation, formal analysis, supervision, and review and editing. D.J.: supervision and review and editing. D.M.: supervision and review and editing. L.V.: conceptualization, supervision, funding acquisition, and review and editing. All authors have read and agreed to the published version of the manuscript.

Notes

The authors declare no competing financial interest.

■ ACKNOWLEDGMENTS

This study was supported by a grant of MUR (Italian Ministry of University and Research) to the Department of Molecular Medicine of the University of Pavia under the initiative "Dipartimenti di Eccellenza (2018-2022) and (2023−2027)". J.C.S. was funded by PNRR the Italian Ministry of University and Research (MUR): ONE HEALTH BASIC AND TRANSLATIONAL RESEARCH ACTIONS (INF-ACT); [number: PE00000007]. D.P. and D.J. acknowledge the Interdepartmental Center "PhotoNext" of Politecnico di Torino for the partial support of this research effort. L.V. and E.R. acknowledge the following members of University of Pavia: Stefano Iervese and Federico Bertoglio for the preliminary microbiological analyses on the biomaterials, Roberta Migliavacca for providing bacterial strains, Lucia Cucca for ICP-OES analysis, Patrizia Vaghi for CLSM analyses (https://cgs.unipv.it/eng/), Giovanna Bruni for EDS-SEM analyses, and Giacomo Dacarro for contact angle measures. Special thanks to Scott Burgess (University of Pavia) for correcting the English of the manuscript.

■ REFERENCES

(1) Pittet, D.; Hugonnet, S.; Harbarth, S.; Mourouga, P.; Sauvan, V.; Touveneau, S.; Perneger, T. V. Effectiveness of a Hospital-Wide Programme to Improve Compliance with Hand Hygiene. *Lancet* **2000**, *356*, 1307−1312.

(2) Campoccia, D.; Montanaro, L.; Arciola, C. R. The Significance of Infection Related to Orthopedic Devices and Issues of Antibiotic Resistance. *Biomaterials* **2006**, *27*, 2331−2339.

(3) Okkeh, M.; Bloise, N.; Restivo, E.; De Vita, L.; Pallavicini, P.; Visai, L. Gold Nanoparticles: Can They Be the Next Magic Bullet for Multidrug-Resistant Bacteria? *Nanomaterials* **2021**, *11*, 312.

(4) Aitken, C.; Jeffries, D. J. Nosocomial Spread of Viral Disease. *Clin. Microbiol. Rev.* **2001**, *14*, 528−546.

(5) Vincent, J.-L.; Bihari, D. J.; Suter, P. M.; Bruining, H. A.; White, J.; Nicolas-Chanoin, M.-H.; Wolff, M.; Spencer, R. C.; Hemmer, M. The Prevalence of Nosocomial Infection in Intensive Care Units in Europe: Results of the European Prevalence of Infection in Intensive Care (EPIC) Study. *J. Am. Med. Assoc.* **1995**, *274*, 639−644.

(6) Bitar, M.; Salih, V.; Mudera, V.; Knowles, J. C.; Lewis, M. P. Soluble Phosphate Glasses: in Vitro Studies using Human Cells of Hard and Soft Tissue Origin. *Biomaterials* **2004**, *25*, 2283−2292.

(7) Islam, M. T.; Felfel, R. M.; Abou Neel, E. A.; Grant, D. M.; Ahmed, I.; Hossain, K. M. Z. Bioactive Calcium Phosphate−Based Glasses and Ceramics and their Biomedical Applications: A Review. *J. Tissue Eng.* **2017**, *8*, No. 2041731417719170.

(8) Podrazký, O.; Peterka, P.; Kašík, I.; Vytykáčová, S.; Proboštová, J.; Mrázek, J.; Kuneš, M.; Závalová, V.; Radochová, V.; Lyutakov, O.; Ceci-Ginistrelli, E.; Pugliese, D.; Boetti, N. G.; Janner, D.; Milanese, D. In Vivo Testing of a Bioresorbable Phosphate-Based Optical Fiber. *J. Biophotonics* **2019**, *12*, No. e201800397.

(9) Bari, A.; Bloise, N.; Fiorilli, S.; Novajra, G.; Vallet-Regí, M.; Bruni, G.; Torres-Pardo, A.; González-Calbet, J. M.; Visai, L.; Vitale-Brovarone, C. Copper-Containing Mesoporous Bioactive Glass Nanoparticles as Multifunctional Agent for Bone Regeneration. *Acta Biomater.* **2017**, *55*, 493−504.

(10) Meena Narayana Menon, D.; Pugliese, D.; Janner, D. Infrared Nanosecond Laser Texturing of Cu-Doped Bioresorbable Calcium Phosphate Glasses. *Appl. Sci.* **2022**, *12*, 3516.

(11) Ceci-Ginistrelli, E.; Pugliese, D.; Boetti, N. G.; Novajra, G.; Ambrosone, A.; Lousteau, J.; Vitale-Brovarone, C.; Abrate, S.; Milanese, D. Novel Biocompatible and Resorbable UV-Transparent Phosphate Glass Based Optical Fiber. *Opt. Mater. Express* **2016**, *6*, 2040−2051.

(12) Gallichi-Nottiani, D.; Pugliese, D.; Boetti, N. G.; Milanese, D.; Janner, D. Toward the Fabrication of Extruded Microstructured Bioresorbable Phosphate Glass Optical Fibers. *Int. J. Appl. Glass Sci.* **2020**, *11*, 632−640.

(13) Ceci-Ginistrelli, E.; Pontremoli, C.; Pugliese, D.; Barbero, N.; Boetti, N. G.; Barolo, C.; Visentin, S.; Milanese, D. Drug Release Kinetics from Biodegradable UV-Transparent Hollow Calcium-Phosphate Glass Fibers. *Mater. Lett.* **2017**, *191*, 116−118.

(14) Sprio, S.; Dapporto, M.; Preti, L.; Mazzoni, E.; Iaquinta, M. R.; Martini, F.; Tognon, M.; Pugno, N. M.; Restivo, E.; Visai, L.; Tampieri, A. Enhancement of the Biological and Mechanical Performances of Sintered Hydroxyapatite by Multiple Ions Doping. *Front. Mater.* **2020**, *7*, 224.

(15) Frei, A.; Verderosa, A. D.; Elliott, A. G.; Zuegg, J.; Blaskovich, M. A. T. Metals to Combat Antimicrobial Resistance. *Nat. Rev. Chem.* **2023**, *7*, 202−224.

(16) Ermini, M. L.; Voliani, V. Antimicrobial Nano-Agents: The Copper Age. *ACS Nano* **2021**, *15*, 6008−6029.

(17) Mitra, D.; Li, M.; Kang, E.-T.; Neoh, K. G. Transparent Copper-Based Antibacterial Coatings with Enhanced Efficacy against *Pseudomonas aeruginosa*. *ACS Appl. Mater. Interfaces* **2019**, *11*, 73−83.

(18) Govind, V.; Bharadwaj, S.; Sai Ganesh, M. R.; Vishnu, J.; Shankar, K. V.; Shankar, B.; Rajesh, R. Antiviral Properties of Copper and its Alloys to Inactivate Covid-19 Virus: a Review. *BioMetals* **2021**, *34*, 1217−1235.

(19) Robinson, J.; Arjunan, A.; Baroutaji, A.; Martí, M.; Tuñón Molina, A.; Serrano-Aroca, Á.; Pollard, A. Additive Manufacturing of Anti-SARS-CoV-2 Copper-Tungsten-Silver Alloy. *Rapid Prototyp. J.* **2021**, *27*, 1831−1849.

(20) Vincent, M.; Duval, R. E.; Hartemann, P.; Engels-Deutsch, M. Contact Killing and Antimicrobial Properties of Copper. *J. Appl. Microbiol.* **2018**, *124*, 1032−1046.

(21) Hutasoit, N.; Kennedy, B.; Hamilton, S.; Luttick, A.; Rahman Rashid, R. A.; Palanisamy, S. Sars-CoV-2 (COVID-19) Inactivation Capability of Copper-Coated Touch Surface Fabricated by Cold-Spray Technology. *Manuf. Lett.* **2020**, *25*, 93−97.

(22) Andreou, A.; Trantza, S.; Filippou, D.; Sipsas, N.; Tsiodras, S. COVID-19: The Potential Role of Copper and N-acetylcysteine (NAC) in a Combination of Candidate Antiviral Treatments Against SARS-CoV-2. *In Vivo* **2020**, *34*, 1567−1588, DOI: 10.21873/invivo.11946.

(23) Alanazi, A. COVID-19 and the Role of Stem Cells. *Regener. Ther.* **2021**, *18*, 334−338.
(24) Rani, I.; Goyal, A.; Bhatnagar, M.; Manhas, S.; Goel, P.; Pal, A.; Prasad, R. Potential Molecular Mechanisms of Zinc- and Copper-Mediated Antiviral Activity on COVID-19. *Nutr. Res. (N.Y.)* **2021**, *92*, 109−128.
(25) Hosseini, M.; Chin, A. W. H.; Behzadinasab, S.; Poon, L. L. M.; Ducker, W. A. Cupric Oxide Coating That Rapidly Reduces Infection by SARS-CoV-2 via Solids. *ACS Appl. Mater. Interfaces* **2021**, *13*, 5919−5928.
(26) Foroutan, F.; McGuire, J.; Gupta, P.; Nikolaou, A.; Kyffin, B. A.; Kelly, N. L.; Hanna, J. V.; Gutierrez-Merino, J.; Knowles, J. C.; Baek, S.-Y.; Velliou, E.; Carta, D. Antibacterial Copper-Doped Calcium Phosphate Glasses for Bone Tissue Regeneration. *ACS Biomater. Sci. Eng.* **2019**, *5*, 6054−6062.
(27) Raja, F. N. S.; Worthington, T.; De Souza, L. P. L.; Hanaei, S. B.; Martin, R. A. Synergistic Antimicrobial Metal Oxide-Doped Phosphate Glasses; a Potential Strategy to Reduce Antimicrobial Resistance and Host Cell Toxicity. *ACS Biomater. Sci. Eng.* **2022**, *8*, 1193−1199.
(28) Grass, G.; Rensing, C.; Solioz, M. Metallic Copper as an Antimicrobial Surface. *Appl. Environ. Microbiol.* **2011**, *77*, 1541−1547.
(29) Di Sieno, L.; Boetti, N. G.; Dalla Mora, A.; Pugliese, D.; Farina, A.; Konugolu Venkata Sekar, S.; Ceci-Ginistrelli, E.; Janner, D.; Pifferi, A.; Milanese, D. Towards the Use of Bioresorbable Fibers in Time-Domain Diffuse Optics. *J. Biophotonics* **2018**, *11*, No. e201600275.
(30) Mussavi Rizi, S. H.; Boetti, N. G.; Pugliese, D.; Janner, D. Phosphate Glass-Based Microstructured Optical Fibers with Hole and Core for Biomedical Applications. *Opt. Mater.* **2022**, *131*, No. 112644.
(31) Rovati, D.; Albini, B.; Galinetto, P.; Grisoli, P.; Bassi, B.; Pallavicini, P.; Dacarro, G.; Taglietti, A. High Stability Thiol-Coated Gold Nanostars Monolayers with Photo-Thermal Antibacterial Activity and Wettability Control. *Nanomaterials* **2019**, *9*, 1288.
(32) Alteri, C.; Cento, V.; Piralla, A.; Costabile, V.; Tallarita, M.; Colagrossi, L.; Renica, S.; Giardina, F.; Novazzi, F.; Gaiarsa, S.; Matarazzo, E.; Antonello, M.; Vismara, C.; Fumagalli, R.; Epis, O. M.; Puoti, M.; Perno, C. F.; Baldanti, F. Genomic Epidemiology of SARS-CoV-2 Reveals Multiple Lineages and Early Spread of SARS-CoV-2 Infections in Lombardy, Italy. *Nat. Commun.* **2021**, *12*, 434.
(33) Reed, L. J.; Muench, H. A Simple Method of Estimating Fifty Percent Endpoints. *Am. J. Hyg.* **1938**, *27*, 493−497.
(34) Martelli, G.; Bloise, N.; Merlettini, A.; Bruni, G.; Visai, L.; Focarete, M. L.; Giacomini, D. Combining Biologically Active β-Lactams Integrin Agonists with Poly(l-lactic acid) Nanofibers: Enhancement of Human Mesenchymal Stem Cell Adhesion. *Biomacromolecules* **2020**, *21*, 1157−1170.
(35) Cochis, A.; Azzimonti, B.; Sorrentino, R.; Della Valle, C.; De Giglio, E.; Bloise, N.; Visai, L.; Bruni, G.; Cometa, S.; Pezzoli, D.; Candiani, G.; Rimondini, L.; Chiesa, R. Data in Support of Gallium (Ga^{3+}) Antibacterial Activities to Counteract *E. coli* and *S. epidermidis* Biofilm Formation onto Pro-Osteointegrative Titanium Surfaces. *Data Brief* **2016**, *6*, 758−762.
(36) Della Valle, C.; Visai, L.; Santin, M.; Cigada, A.; Candiani, G.; Pezzoli, D.; Arciola, C. R.; Imbriani, M.; Chiesa, R. A Novel Antibacterial Modification Treatment of Titanium Capable to Improve Osseointegration. *Int. J. Artif. Organs* **2012**, *35*, 864−875.
(37) Pimenta de Melo, L.; Contessi Negrini, N.; Farè, S.; de Mello Roesler, C. R.; de Mello Gindri, I.; Salmoria, G. V. Thermomechanical and In Vitro Biological Characterization of Injection-Molded PLGA Craniofacial Plates. *J. Appl. Biomater. Funct. Mater.* **2019**, *17*, No. 2280800019831599.
(38) Gatto, M. L.; Groppo, R.; Bloise, N.; Fassina, L.; Visai, L.; Galati, M.; Iuliano, L.; Mengucci, P. Topological, Mechanical and Biological Properties of Ti6Al4V Scaffolds for Bone Tissue Regeneration Fabricated with Reused Powders via Electron Beam Melting. *Materials* **2021**, *14*, 224.
(39) Ceccarelli, G.; Bloise, N.; Mantelli, M.; Gastaldi, G.; Fassina, L.; De Angelis, M. G. C.; Ferrari, D.; Imbriani, M.; Visai, L. A Comparative Analysis of the *In Vitro* Effects of Pulsed Electromagnetic Field Treatment on Osteogenic Differentiation of Two Different Mesenchymal Cell Lineages. *Biores. Open Access* **2013**, *2*, 283−294.
(40) Bloise, N.; Massironi, A.; Della Pina, C.; Alongi, J.; Siciliani, S.; Manfredi, A.; Biggiogera, M.; Rossi, M.; Ferruti, P.; Ranucci, E.; Visai, L. Extra-Small Gold Nanospheres Decorated With a Thiol Functionalized Biodegradable and Biocompatible Linear Polyamidoamine as Nanovectors of Anticancer Molecules. *Front. Bioeng. Biotechnol.* **2020**, *8*, 132.
(41) Saino, E.; Maliardi, V.; Quartarone, E.; Fassina, L.; Benedetti, L.; De Angelis, M. G. C.; Mustarelli, P.; Facchini, A.; Visai, L. In Vitro Enhancement of SAOS-2 Cell Calcified Matrix Deposition onto Radio Frequency Magnetron Sputtered Bioglass-Coated Titanium Scaffolds. *Tissue Eng. Part A* **2010**, *16*, 995−1008.
(42) Bloise, N.; Patrucco, A.; Bruni, G.; Montagna, G.; Caringella, R.; Fassina, L.; Tonin, C.; Visai, L. In Vitro Production of Calcified Bone Matrix onto Wool Keratin Scaffolds via Osteogenic Factors and Electromagnetic Stimulus. *Materials* **2020**, *13*, 3052.
(43) Dapporto, M.; Tavoni, M.; Restivo, E.; Carella, F.; Bruni, G.; Mercatali, L.; Visai, L.; Tampieri, A.; Iafisco, M.; Sprio, S. Strontium-Doped Apatitic Bone Cements with Tunable Antibacterial and Antibiofilm Ability. *Front. Bioeng. Biotechnol.* **2022**, *10*, No. 969641.
(44) Cai, S.; Wu, C.; Yang, W.; Liang, W.; Yu, H.; Liu, L. Recent Advance in Surface Modification for Regulating Cell Adhesion and Behaviors. *Nanotechnol. Rev.* **2020**, *9*, 971−989.
(45) Karadjian, M.; Essers, C.; Tsitlakidis, S.; Reible, B.; Moghaddam, A.; Boccaccini, A. R.; Westhauser, F. Biological Properties of Calcium Phosphate Bioactive Glass Composite Bone Substitutes: Current Experimental Evidence. *Int. J. Mol. Sci.* **2019**, *20*, 305.
(46) Kaur, G.; Pandey, O. P.; Singh, K.; Homa, D.; Scott, B.; Pickrell, G. A Review of Bioactive Glasses: Their Structure, properties, Fabrication and Apatite Formation. *J. Biomed. Mater. Res. Part A* **2014**, *102*, 254−274.
(47) Erol, M. M.; Mouriño, V.; Newby, P.; Chatzistavrou, X.; Roether, J. A.; Hupa, L.; Boccaccini, A. R. Copper-Releasing, Boron-Containing Bioactive Glass-Based Scaffolds Coated with Alginate for Bone Tissue Engineering. *Acta Biomater.* **2012**, *8*, 792−801.
(48) Kargozar, S.; Mozafari, M.; Ghodrat, S.; Fiume, E.; Baino, F. Copper-containing bioactive glasses and glass-ceramics: From tissue regeneration to cancer therapeutic strategies. *Mater. Sci. Eng. C* **2021**, *121*, No. 111741.
(49) Gérard, C.; Bordeleau, L. J.; Barralet, J.; Doillon, C. The stimulation of angiogenesis and collagen deposition by copper. *Biomaterials* **2010**, *31*, 824−831.
(50) Azizi, A.; Turkki, P.; Huynh, N.; Massera, J.; Hytönen, V. Surface Modification of Bioactive Glass Promotes Cell Attachment and Spreading. *ACS Omega* **2021**, *6*, 22635−22642.
(51) Hu, S.; Chang, J.; Liu, M.; Ning, C. Study on Antibacterial Effect of 45S5 Bioglass. *J. Mater. Sci. Mater. Med.* **2009**, *20*, 281−286.
(52) Salah, I.; Parkin, I. P.; Allan, E. Copper as an Antimicrobial Agent: Recent Advances. *RSC Adv.* **2021**, *11*, 18179−18186.
(53) Delumeau, L. V.; Asgarimoghaddam, H.; Alkie, T.; Jones, A.; Lum, S.; Mistry, K.; Aucoin, M.; DeWitte-Orr, S.; Musselman, K. Effectiveness of antiviral metal and metal oxide thin-film coatings against human coronavirus 229E. *APL Mater.* **2021**, *9*, 111114.
(54) Xie, Y.; Guo, W.; Lopez-Hernadez, A.; Teng, S.; Li, L. The pH Effects on SARS-CoV and SARS-CoV-2 Spike Proteins in the Process of Binding to hACE2. *Pathogens* **2022**, *11*, 238.
(55) Adamczyk, Z.; Batys, P.; Barbasz, J. SARS-CoV-2 Virion Physicochemical Characteristics Pertinent to Abiotic Substrate Attachment. *Curr. Opin. Colloid Interface Sci.* **2021**, *55*, No. 101466.
(56) Krebs, F.; Scheller, C.; Grove-Heike, K.; Pohl, L.; Wätzig, H. Isoelectric Point Determination by Imaged CIEF of Commercially Available SARS-CoV-2 Proteins and the hACE2 Receptor. *Electrophoresis* **2021**, *42*, 687−692.
(57) Dasan, A.; Chandrasekar, A. Special Issue: Bioceramics, Bioglasses, and Gels for Tissue Engineering. *Gels* **2023**, *9*, 586.

https://doi.org/10.1021/acsomega.3c04293
ACS Omega 2023, 8, 42264−42274